Journal of Power Sources 570 (2023) 233064

Contents lists available at ScienceDirect

Journal of Power Sources

journal homepage: www.elsevier.com/locate/jpowsour

In-situ measurement of internal gas pressure within cylindrical lithium-ion cells

B. Gulsoy *, T.A. Vincent, C. Briggs, J.E.H. Sansom, J. Marco

WMG, University of Warwick, Coventry, CV4 7AL, United Kingdom

HIGHLIGHTS

- New methodology to measure in-situ gas pressure within commercial cylindrical cells.
- In cell gas accumulation due to electrical, thermal loading and ageing quantified.
- New insights into reversible and irreversible gas pressure changes are presented.
- Pressure accumulation during ageing correlated with battery state of health (SOH).

ARTICLE INFO

Keywords:
Lithium-ion batteries
Cell instrumentation
Gas pressure
In-situ monitoring
Ageing
Advanced characterization
Cell-sensing

ABSTRACT

Internal gas pressure is a key parameter that varies depending on cell heating and gas formation over the lifetime of a lithium-ion cell under dynamic load conditions and ageing. In our research, for the first time, we present a methodology to directly measure internal gas pressure during pre-instrumentation, cell operation and ageing via an embedded sensor system. Cylindrical format cells (LG-INR21700M50) are instrumented using our proven instrumentation technique. Our study demonstrates that the performance and degradation of instrumented cells are not adversely affected by the instrumentation process. In this study, the effect of state-of-charge (SOC), degradation and temperature on internal gas pressure is evaluated. Initial results highlight a nonlinear relationship between gas pressure and SOC of the cells during charging and discharging and, gas pressure and temperature when the cells are operated under no-load conditions. Our study further highlights that gas pressure accumulation can be correlated with capacity fade or state-of-health (SOH). Monitoring of internal gas pressure could therefore become a useful additional indicator of SOC and SOH and provide new insights into degradation and the safety of lithium-ion cells.

1. Introduction

Over the last two decades, the demands for energy storage units have increased exponentially with the proliferation of portable electronics. This demand continues to expand with new electrification targets to replace fossil fuels in multiple applications such as hybrid electric vehicles, full electric vehicles, electric aircrafts, grid-connected energy storage, and renewable energy systems. Lithium-ion batteries (LIBs) are considered to be one of the most promising electrochemical storage devices due to their comparatively high gravimetric and volumetric energy/power, high voltage, absence of severe memory effects, and long cycle life [1–3]. However, there are major challenges associated with the practical application of LIBs in terms of monitoring and controlling of the battery status, such as state-of-health (SOH), state-of-charge (SOC), power capacity, internal temperature and internal gas pressure. The poor monitoring of battery systems could cause degenerative and faster degradation, decreasing performance and potential catastrophic failures of LIBs and LIB-powered systems. This insufficiency could create a major challenge for large-scale applications for aerospace and automotive industries where improved safety, longer cycle life, extended capacity, and fast-charging requirements are highly demanded [3–5].

Battery management systems (BMS) play a critical role in terms of the safety, reliability, efficiency, and longevity of LIB systems. However, existing BMS are still insufficient to meet the demand for advanced monitoring and control for LIB systems. Since BMS typically relies on very limited measurements of current, terminal voltage and surface temperature of the modules inside a battery pack. For example, the

* Corresponding author.
E-mail address: begum.gulsoy.1@warwick.ac.uk (B. Gulsoy).

https://doi.org/10.1016/j.jpowsour.2023.233064
Received 19 January 2023; Received in revised form 20 March 2023; Accepted 6 April 2023
Available online 15 April 2023

Abbreviations

OCV	open circuit voltage
SOC	state of charge
SOH	state of health
BMS	battery management system
LIB	lithium-ion batteries
Z	internal impedance
CT	x-ray computed tomography
RPT	reference performance test
DC	direct current
DCIR	direct current internal resistance
CC	constant current
CV	constant voltage
NMC	nickel manganese cobalt
LTO	lithium titanate oxide
CID	current interrupt device

surface temperature of the batteries is typically measured at module-level with different manufacturers and integrators adopting different approaches to instrumentation accommodated in a few different locations in the battery assembly. As highlighted in our previous research [6], there is a significant difference between the surface and internal (core) temperature of a single cell. Hence, our understanding of the internal temperature changes of an individual cell inside a battery pack is limited [7]. To the authors' knowledge, there are no commercial BMS with pressure sensor interface capability. We propose that the measurement of temperature and pressure is essential to understand the SOH of a cell. Current BMS techniques, reliant on model prediction, fail to accurately represent the physical failure mechanisms of the cell. The accuracy of these models is tied to the original experimental datasets, which are inherently linked to the cell chemistry and format. Cell ageing in end-applications cannot be accurately predicted without sensor data, thus the ability of the BMS to manage the pack lessens as the pack ages. To remedy such deficiencies and limitations requires the advances in the monitoring and control functions of the BMS. This potentially raises the need for cell-level sensing, which could provide more in-depth knowledge of real-time cell status, and underpins the measurement of new battery parameters, such as core temperature, internal gas pressure, heat distribution, strain, and electrode voltage. This helps to satisfy the urgent expectations of improving battery safety, performance and lifetime [3].

Gas generation during lithium-ion battery operation is known to be a complex phenomenon. It is dependent on various parameters such as the composition of electrolyte, the nature of electrodes, cycling and operating conditions, e.g., cut-off voltage and temperature. More importantly, the gases that have been produced during battery operation and storage accumulate inside sealed lithium-ion batteries. The gas accumulation is primarily localised at particularly areas such as the electrode/electrolyte interfaces [8]. This results in an increase in the electrical resistance of the cell [9], causing further heat generation and consequently the loss in the electrochemical performance of the cell [10]. This also results in an increase in internal pressure leading to mechanical stress on the electrode materials, causing faster ageing and potential safety concerns. The pressure increase can also change the physical structure of the batteries which have a softer case, e.g., pouch cells [11]. For example, sweeling ranging from 6% to 20% is observed in commercial pouch cells after being stored at high temperatures [12], whereas the physical changes in cylindrical cell housing are unlikely due to the rigidity of the cell structure [11].

An improved understanding of internal pressure within a LIB cell enhances our understanding of cell design and safe operation. Thermal runaway and mechanical failure, such as side wall rupture, have been widely reported in the literature [13,14], with many articles further discussing the implications of cell failure at a system-scale and the need for different mitigation strategies. Novel cell designs and the use of in-built features such as a current interrupt device (CID) are employed to reduce the severity of cell failure. The ability to accurately measure internal pressure, in a repeatable manner, is a pre-requisite for the validation of such components and could underpin future innovations in cell design and LIB safety.

Since the indication of gas pressure increase within lithium-ion cells is very limited, a number of authors [15–18] have reported experiments where the gas pressure inside lithium-ion cells has been monitored. In the literature, there are different approaches presented to monitor gas pressure under cell operation. Matasso et al. [15] constructed a test chamber in order to examine the gas pressure and gas formation of a cylindrical lithium-ion battery with lithium cobalt oxide cathode [15]. In their test setup, the pressure vent cap was removed from the cell. Afterwards, it was transferred into their sealed test chamber. The significant increase in gas pressure was observed over the 250 cycles. The authors indicated that the rate of pressure increase per cycle was decreased when the cell aged. They found that the rate of pressure increase is dependent on the cycling rate. Schiele et al. [16] developed a multichannel pressure-measurement system to monitor the pressure inside a self-built cells. They observed significant gas formation during formation cycling. It was highlighted that gas formation was higher at elevated temperatures. They also correlated the capacity loss during the formation process with the pressure increases due to gassing [16]. Schweidler et al. [17] used the same experimental setup with Schiele et al. and monitored the gas pressure of lithium titanate oxide (LTO)/graphite cells during electrical cycling. The pressure increases due to gassing and the change in the volume of graphite was found where the volume changes in the LTO were considered negligible [17]. Schmitt et al. [18] used custom-built prismatic cells in order to monitor the gas pressure over 1000 cycles. They integrated a commercially available pressure sensor into their custom-built cells. They found an irreversible pressure increase after a long period of electrical cycling, which they interpreted as due to gas formation. The authors correlated the pressure increases with the loss of energy capacity due to the degradation of the cell. They also investigated the SOC and temperature effects on gas pressure changes. Their results indicated that both SOC and temperature are a nonlinear relationship with the gas pressure [18].

Internal gas pressure is one of the important battery parameters that vary depending on the heating effect and gas formation over the lifetime of a lithium-ion cell under dynamic load conditions and ageing. This could be a promising parameter to measure since gas pressure can provide valuable information on battery performance, lifetime, and safety for large-scale applications, where more in-depth knowledge is required. In this study, we developed an individual cell-sensing method for 21,700 format cylindrical cells to monitor internal gas pressure changes during cell operation and storage. Here, we demonstrate our advanced cell-sensing method, presented in [6], is well suited for instrumentation of pressure transducers. Our methodology for monitoring internal pressure changes in this study advances the techniques previously described in the literature. Namely, offering a repeatable instrumentation method, compatible with commercial cells relevant to the automotive and aerospace industry, minimal damage to the cell structure which we believe allows the cell to retain the same limits of operation specified by the manufacturer. In this work, direct measurement of the gas pressure was investigated for cylindrical cells during operation, and the effect of the cell state-of-charge (SOC), degradation and temperature on gas pressure inside the cells are evaluated.

The structure of this paper as follows. Experimental methodology is presented in Section 2, which discusses the experimental setup for pre-instrumentation pressure, cell instrumentation, verification, and electrochemical tests performed. Results and discussion are presented in Section 3. Further work and Conclusion are discussed in Sections 4 and 5 respectively.

2. Experimental methodology

2.1. Experimental test setup

In this study, commercial 21,700 format cells were employed to monitor the gas pressure inside a cylindrical cell. These cells were manufactured by LG Chem and comprise an NMC 811 formulation for the cathode and a Graphite-SiO_x anode. The gas pressure was investigated for three experimental conditions: (i) pre-instrumentation, (ii) typical cell operation and (iii) ageing through extended charge-throughput. The flow diagram of the experimental tests conducted in this study are summarised in Fig. 1. Monitoring of gas pressure at pre-instrumentation was investigated within three pristine/new cells. This initial experiment was conducted within a bespoke battery abuse test facility within the university via a method of LIB penetration testing. Afterwards, a new set of three pristine cells were instrumented with pressure sensors for the investigation of gas pressure changes during cell operation and ageing. The characterisation tests included a reference performance test (RPT), electrical cycling. The application of temperature profiles was also performed within a climate chamber (Binder MKF56) using a Bio-Logic VSP-300 Potentiostat with the cell at no-load. For all experiments, the cell surface temperature was monitored via K-type thermocouples attached to the centre location of the cell. The temperature data was logged at a sample frequency of 10 Hz using a data logger (PicoLog TC-08). Details of the experimental setup and individual experimental procedures are provided in the following sections.

2.2. Pre-instrumentation gas pressure

The purpose of this initial experiment is to quantify the inherent pressure within the LIB as a result of formation cycles and initial SOC conditioning by the manufacturer for storage and transport. Electrical pre-conditioning of the three pristine cells was avoided. The cells were kept inside the climate chamber (set to 25 °C) for a period of 2 h for

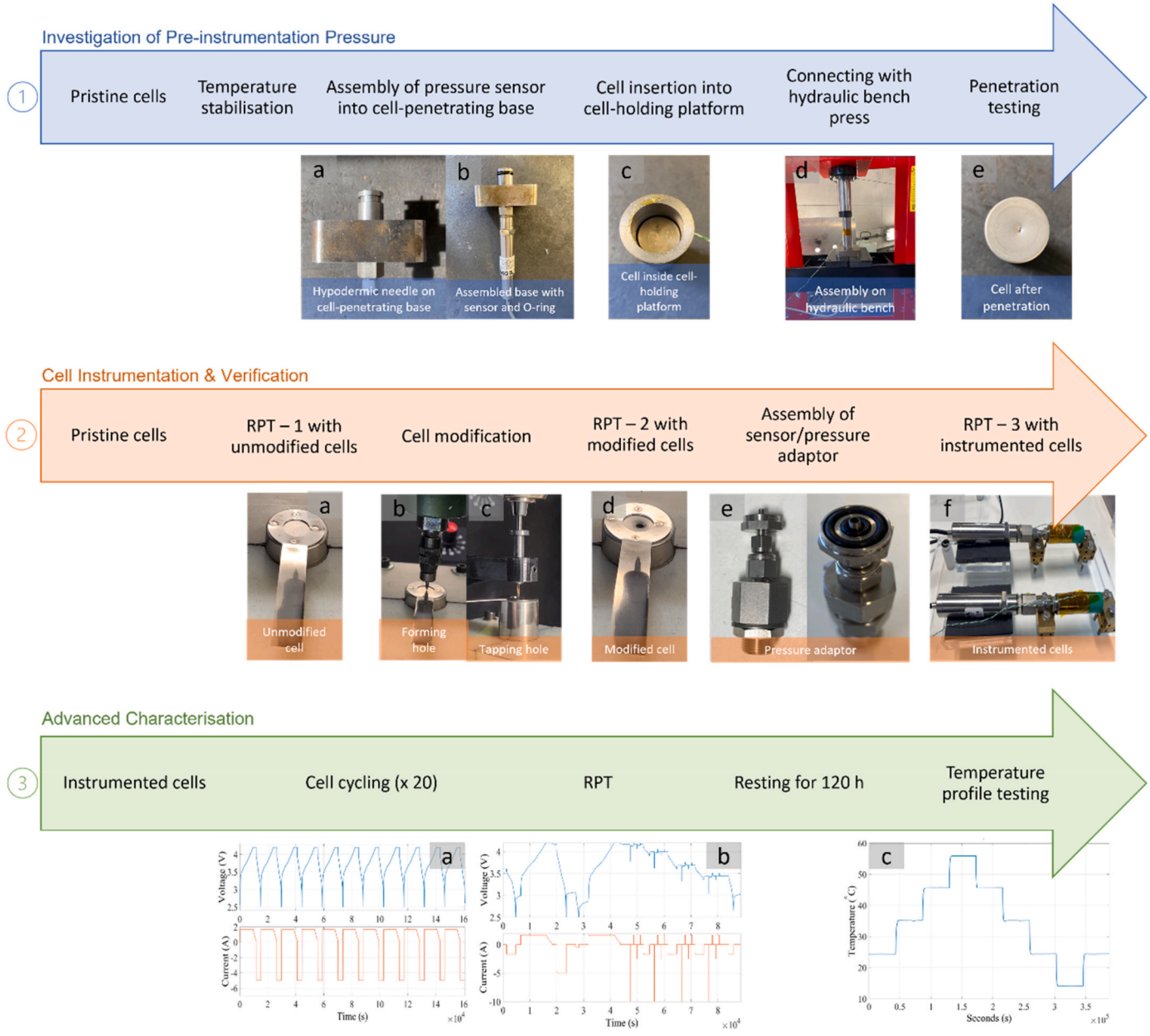

Fig. 1. Experimental flow diagram including pre-instrumentation pressure investigation, cell instrumentation and verification/characterisation tests performed in this work.

temperature stabilisation before the penetration testing. The SOC level for the cells was 30% SOC (post-manufacturing delivery condition) during testing.

Pre-instrumentation pressure was measured during bespoke penetration testing. A test rig that comprised a cell-holding platform, Fig. 1 (1c), and cell-penetrating base, Fig. 1(1a), was designed in order to open the negative terminal of the cell with a bespoke hypodermic needle. The needle was connected to a pressure transducer, where the needle formed a small passage to the core of the cell. The hole on the negative terminal after penetration test is shown in Fig. 1(1e). Penetration was conducted with a hydraulic bench press (Clarke CSA10BB) as shown in Fig. 1(1d). During testing, hydraulic pressure was slowly applied to the cells, and the internal gas of the cell was released through the needle. The gas pressure was monitored via the pressure transducer (Gauge digital pressure transducer operates up 7 bar, with an accuracy of ±0.20% full scale deflection, MM-G-100-USBH-B-4-MD-0-T8-A3-CE, Omega). For precise gas pressure measurements, the cell-holding platform was designed to have a low-volume path during the penetration movement which is from the needle's initial position to the later state that forms a small passage. The volume change inside the cell-holding platform was calculated as 0.767 cm^3. Additionally, the base plate was supported with O-rings and bonded washers to avoid gas leakage. The penetration testing was conducted at 22.5°C (±0.3°C) of ambient temperature. The images of testing rig are shown in Fig. 1(1).

2.3. Cell instrumentation with pressure sensor

Modifying the LIB cell to monitor the gas pressure inside the cylindrical cell was achieved by extending our previously reported cell instrumentation method [6], which was based on creating a pilot hole on the negative terminal using a flow-drill method to avoid swarf formation and material loss. The working principle of the flow-drill was to form a hole through a high-speed rotation and the instantaneous generation of heat. This combined with an appropriate feed rate formed a hole with minimal damage and swarf on the negative terminal. While forming the hole, a burr inside the hollow core is created, where the current collector and the cell were joined. This burr was used a create threads for resealing the cell after instrumentation. This method enables access directly into the hollow mandrel of the cylindrical cell without causing mechanical damage to the integrity of the cell case or its internal components. Additionally, it has benefits of creating a secure and repeatable method of fitting the sensors.

For this research, three cylindrical cells were discharged to 3 V (less than 20% SOC) at a constant current rate of C/3 prior to cell modification. Afterwards, a pilot hole located in the centre of the negative terminal was formed with a diameter of 1.8 mm. This is followed by a thread forming procedure to create an M 2.5 thread on the internal burr. As a final stage of cell modification, the cells were temporarily re-sealed within a bonded washer and nylon screw to perform a performance characterisation test (further details are provided in Section 2.4) until the sensor assembly process.

To monitor gas pressure changes under nominal cell operation, digital gauge pressure transducers from Omega were used. The sensors have a high accuracy of ±0.20% throughout the range of 7 bar with a USB data output. A bespoke fitting to interface to the hollow mandrel core with an external pressure transducer was designed and fabricated using gas-tight tube fittings (SS1001OR, SS201PC and SS20074RG, Swagelok). The parallel thread of Swagelok SS1001OR was replaced with a threaded bulged tube, and a groove was created for the second O-ring (FKM 3 mm bore with 6 mm OD, RS Pro) to reseal the cell after instrumentation. Afterwards, SS1001OR was assembled with SS20074RG through SS201PC. This gas transfer piece from the hollow mandrel core to the transducer is named as the *pressure adaptor* in this paper. The adaptor has been designed to fit any G ¼ inch female pressure sensor, which allows for the use of different sensor types to be selected for nominal cell operation or battery abuse test conditions. The pressure adaptor and the assembly with pressure transducer are shown in Fig. 1 (2e) and Fig. 1(2f) respectively.

Prior to instrumentation, the sealing quality of the pressure adaptors was verified by a pressure leak test. The testing was performed using a leak test panel from JW Froehlich (MPS200). After the pressure transducers were assembled with the adaptors, they were individually connected to the test panel and pressurised to 2.5 bar (deemed to be representative of the highest likely pressure the cell would experience during typical operation based on previous studies [18,19]) via a compressor (Bambi 75/250). For each pressure adaptor, the leak test was repeated five times and the average volume of leakage was calculated as 12 Pa over a measurement period of 8.5 s. The leakage was less than 15 Pa (0.15 mbar) was accepted as a successful seal. Afterwards, all pressure transducers were recalibrated in the range of 50 mbar to 2.5 bar at several calibration points (10 mbar, 50 mbar, 100 mbar, 200 mbar, 500 mbar, 1 bar, 1.5 bar, 2 bar and 2.5 bar) using a pressure calibrator (Druck DPI612 Flex). A linear calibration curve for all pressure sensors was observed in line with the manufacturer's specification.

The integration of pressure transducers with the modified cells was performed inside a glovebox, where the ambient pressure was between 2 mbar and 3 mbar, and O_2 and H_2O concentrations were maintained below 0.1 ppm. With the temporary seal removed, the pressure adaptor was positioned perpendicular to the negative terminal and screwed into the cell body to re-seal the cell. A typical instrumented cell with a pressure transducer was shown in Fig. 1(2f).

2.4. Reference performance test (RPT)

The electrochemical performance of the instrumented cells was verified using a reference performance test (RPT). In order to identify the occurrence of any detrimental effect of the instrumentation process on cell performance, discharge capacity and DC internal resistance (DCIR) were measured at each instrumentation stage, as defined in our previous article [6]. These were (i) on the pristine condition before any cell modification, (ii) after the cells were engineered, and (iii) after assembly of sensor and resealing. This performance characterisation procedure comprised a constant-current – constant-voltage (CC-CV) measure of energy capacity at current magnitudes of 1C and C/10. The constant-voltage occurred at 4.2 V until the value of current reduced below C/20. The power capability was evaluated through the sequence of pulse discharges, in which current magnitudes of 2C and C/2 were applied for 10 s at SOC levels of 100%, 80%, 50% and 20%. The RPT testing profile is shown in Fig. 1(3b).

During the 3rd stage of the performance characterisation tests, gas pressure changes inside the instrumented cells were monitored to observe the relationship between SOC and gas pressure. Pressure data from digital transducers was logged using the manufacturer's bespoke data logging software (Omega Digital Transducer Application) at a sample frequency of 10 kHz. All performance characterisation experiments were performed inside a climate chamber set to 25 °C, and prior to each testing, the cells were placed in the chamber for 2 h to allow them to reach thermal equilibrium.

2.5. Cycling

The potential for the instrumented cells to generate higher gas pressure during ageing was investigated by ageing the LIBs through continuous electrical loading. The cells were repeatedly electrically loaded for 100 cycles, and gas pressure changes inside the cells monitored. Additionally, the reduction in retained energy capacity and change in DC internal resistance (DCIR) of the instrumented cells was quantified via an RPT, which was repeated after the 20th, 40th, 60th, 80th and 100th cycles. These values were compared with the reference cells' from our previously published study [6] to investigate the relative degradation characteristics and if there is any difference in ageing due to the instrumentation process.

During ageing, charge and discharge rates of C/3 and 1C were employed respectively. All instrumented cells were charged to the upper voltage limits of 4.2 V using a CC-CV procedure. The CV stage was terminated when the applied current reduced below C/20. During discharging stage, a CC current was applied to the cells until a lower cut-off voltage of 2.5 V was reached. A duration of 1s was allowed between each charge-discharge cycle. The cycling profile was applied to the instrumented cells is shown in Fig. 1(3a). All ageing cycling and RPT were conducted inside the climate chamber set to 25 °C.

After ageing cycling was completed, all instrumented cells were kept at no-load during the period of 120 h inside climatic chamber at the same environmental conditions (25 °C) to observe any irreversible changes in gas pressure.

2.6. Temperature profiles

Before understanding in-operando gas pressure changes, the influence of temperature on gas pressure inside the cells were investigated using temperature profile testing. The volume changes were considered negligible for cylindrical cells during cell cycling due to the rigidity of the cell structure. Thus, internal pressure inside the cell is expected to increase because of gas formation and the temperature rise, according to the ideal gas law given as:

$$P \times V = n \times R \times T \quad \text{(Eq. 1)}$$

where P is the absolute pressure of the gas, V is the gas volume, n is the amount of substance of gas or number of moles, R is the universal gas constant, 8.3145 J/mol K, and T is the absolute temperature of the gas. For the instrumented cells, the volume in (Eq. (1)) is calculated as the sum of the available volume inside the cell and pressure adaptor.

During these validation tests, the instrumented cells were under open-circuit conditions while the ambient temperature was changed inside the climate chamber. The ambient temperature of the cells was set to different temperature levels where they were held constant for a period of 12 h. The ambient temperature (T_{amb}) was set in the order of $25, 35, 45, 55, 45, 35, 25, 15, 25$ ° C as shown in Fig. 1(3c). Gas pressure changes inside the cells and surface temperature of the cells were monitored during temperature profile testing.

3. Results and discussion

3.1. Understanding pre-instrumentation gas pressure

Fig. 2 illustrates the pressure increase inside cell-holding platform for each cell under test and the associated cell surface temperature measured during testing. From time t = 0, through to 15s, the pressure gradually increased due to the volume change during penetration movement, which is from the needle's initial position to the later state that forms a small passage. Once the needle breaks through the negative terminal of the cell (at t = 15 s), a significant rise in the pressure was observed for all the cells. Since the volume change inside the cell was negligible during penetration testing, e.g., less than 1.15 mm^3, this sudden change in pressure reading corresponds to the internal cell pressure, *pre-instrumentation gas pressure*. The pre-instrumentation pressure of *Cell A*, *Cell B* and *Cell C* are shown in Fig. 2 (a) as df_A, df_B and df_C respectively, and these measurements are tabulated in Table 1. This provides greater insight into the gas pressure created during formation cycles and post-manufacturing. As can be seen from the tabulated results, approximately 260 mbar gas pressure was observed after formation and post-manufacturing.

3.2. Performance and degradation characteristics of instrumented cells

Fig. 3(a) illustrates the effects of cell instrumentation on cell performance, in terms of discharge energy capacity measured from each RPT test during the instrumentation process. The median discharge capacity of the three cells was found to be 4.806 Ah at the unmodified or *pristine* stage. A negligible capacity drop was observed after the cell modification and instrumentation stages. The discharge capacity of three modified and instrumented cells were found to be 4.793 Ah and

Table 1
Gas pressure at pre-instrumentation condition measured during the penetration testing.

Cell Names	Pre-Instrumentation Pressure (mbar)	Cell Surface Temperature (°C)
Cell A	264.54	22.50
Cell B	247.23	22.41
Cell C	268.08	22.33

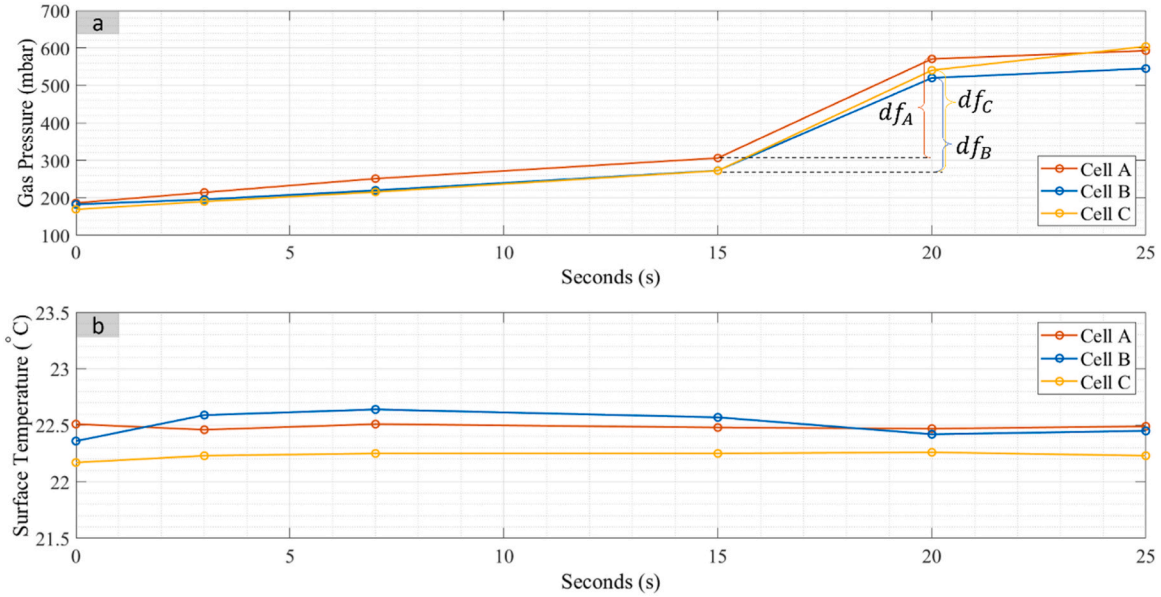

Fig. 2. (a) Pressure inside the cell-holding platform and (b) cell surface temperature during penetration testing.

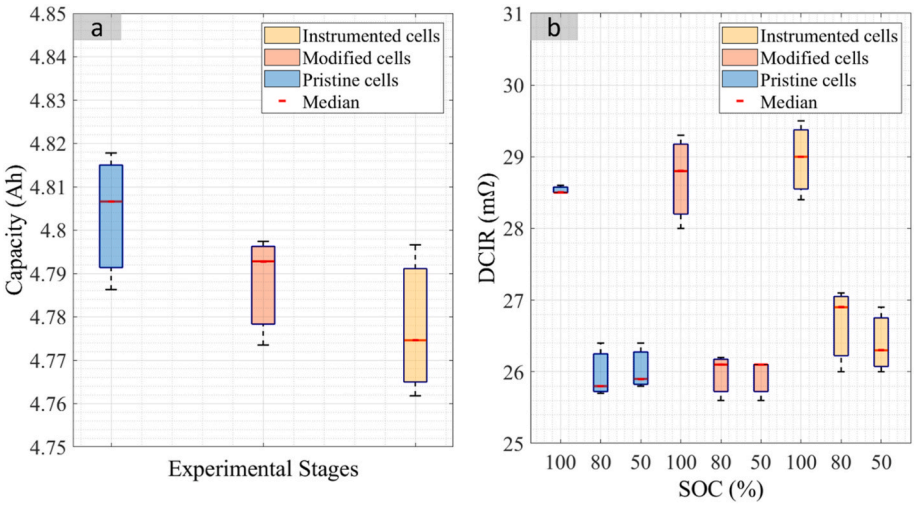

Fig. 3. (a) Energy capacity and (b) DC internal resistance changes at each cell instrumentation stage.

4.775 Ah respectively, which corresponds to a decrease of 0.27% and 0.65% in the initial capacity.

To understand the effect of cell modification (e.g., forming a tapped hole in the current collector), sensor insertion and sealing processes, the DCIR of all cells were obtained at a 2C pulse discharge test from RPT during the instrumentation process. Fig. 3(b) summarises the variations in measured DCIR at 100% 80% and 50% SOC. The median DCIR of the three cells was found to be 28.5 mΩ at 100% SOC, 25.8 mΩ at 80% SOC and 25.9 mΩ at 50% SOC for the pristine stage. A small increase was found in the DCIR values after cell modification and instrumentation. These results are consistent with those observed in our previous work [6]. The maximum increase in measured DCIR was observed as 0.5 mΩ at 100% SOC, 1.1 mΩ at 80% SOC and 0.4 mΩ at 50% SOC. During the cell modification process, an average 4.91 mm^2 decrease in the surface area of the current collector, which was linked to the cell can, was observed. The decrease in the contact area was identified via computed tomography in our previously published article [6], and confirmed that it corresponds with the observed rise in DCIR.

The consistency in the discharge capacity and DCIR values between pristine and instrumented cells indicates that the electrochemical performance of the cells has not been impacted by the cell modification, sensor insertion and sealing processes. Additionally, the similarities between the results published previously [6] and recent findings further reaffirm the repeatability of cell instrumentation procedure.

The effect of cell instrumentation on ageing characteristics is summarised in Fig. 4. The relative reduction in energy capacity and the variation in DCIR of both instrumented and reference cells are shown in Fig. 4 (a) and Fig. 4 (b) over 100 cycles, respectively. For the instrumented cells, the discharged capacity after instrumentation was considered as initial cell capacity (e.g., 100%), whereas the discharge capacity at pristine stage was used for the reference cells as described in [6]. The initial energy capacity of the instrumented and reference cells was 4.78 Ah and 4.83 Ah, respectively. As highlighted by Fig. 4 (a) the capacity fade was found to be 5.1%, 4.7% and 5.4% for the instrumented cells, *Cell 1*, *Cell 2* and *Cell 3* respectively, after 100 cycles. Conversely, this value was found to be 5.3% for the reference cells. The comparison of the capacity fade between the instrumented and reference cells indicates that the ageing characteristics of the cells has not been affected by the cell instrumentation procedure. Similar results were also observed from the variation of DCIR at 100% SOC over 100 cycles. Fig. 4 (b) illustrates that the median DCIR of reference cells has increased by 3.1 mΩ after 100 cycles due to cell ageing. For the instrumented cells, this increase in the DCIR was found to be 2.9 mΩ for *Cell 1* and 2.7 mΩ for *Cell 2* and *Cell 3*. However, a noticeable difference in DCIR values was observed between instrumented and reference cells at the beginning of the cycling, as 1.3 mΩ for *Cell 1* and *Cell 2*, and 1.5 mΩ for *Cell 3*.

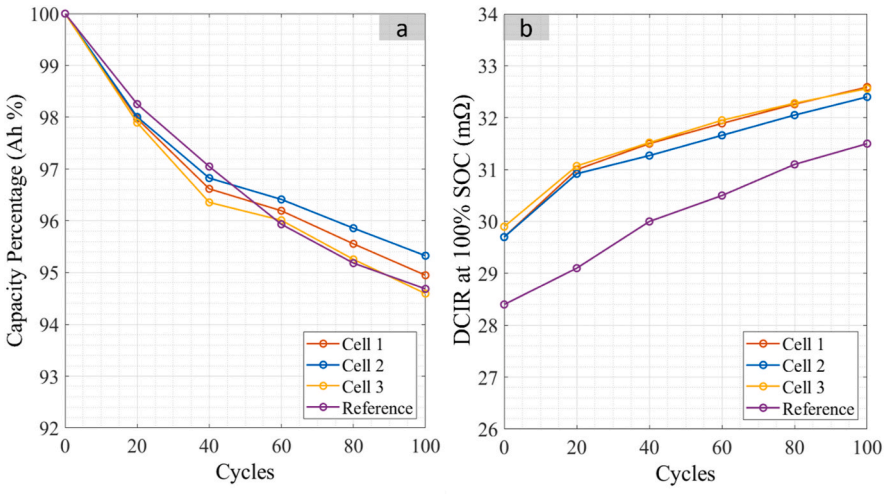

Fig. 4. (a) Energy capacity and (b) DC internal resistance changes of pressure sensor instrumented cells during 100 cycles.

3.3. Gas pressure changes dependent on SOC (%)

The influence of the SOC (%) on gas pressure inside the cells was investigated. The pressure measurements were taken for several SOC levels and different ageing conditions during the charging and discharging processes as defined earlier. Fig. 5 illustrates the gas pressure variation dependent on SOC. The variation in gas pressure (ΔP) at different SOC levels was calculated against the pressure measured at 0% SOC. For the different ageing conditions, the results of the RPT tests that were performed after instrumentation, after 20 cycles, and after 100 cycles were used for the analysis of pressure dependence a on the SOC. These conditions were named as '*INS*','*A20C*' and '*A100C*' respectively, in Fig. 5.

A nonlinear relationship between the gas pressure and SOC was observed during the charging and discharging processes. No significant pressure changes were observed during the charging process between 0% SOC and 30% SOC. This was followed by different gradients of increases which were almost linear. The pressure growth between 30% and 90% SOC was much higher than that after 90% SOC. Conversely, the pressure changes during the discharge process had a different characteristic behaviour. A steady increase was observed from 0% SOC to 70% SOC for the cells after instrumentation, but this was extended to 90% SOC after the cells were aged with 100 cycles. After that, a drop of 25 mbar was observed.

As highlighted in Fig. 5 (a) and (b), the internal pressure was slightly increased when the cell is aged during the discharge process. This pressure rise was measured at nearly 10 mbar at lower SOC, e.g., less than 60% SOC during discharging. When the cells are aged, the maximum pressure increase was observed at 90% SOC. However, there was a small pressure accumulation due to ageing during the charging stage. e.g., less than 5 mbar comparing the pressure in A20C and A100C.

3.4. Irreversible gas pressure accumulation during cell ageing

Fig. 6 illustrates the gas pressure accumulation inside the cells during cell cycling. An increase of 50 mbar (peak) in the pressure was observed for all cells from the beginning of cycling. It is believed that this was caused by the elevated cell temperature due to the applied current during the charging and discharging processes. The monotonically increasing pressure is superimposed on a cyclic variation in pressure, of approximately 100 mbar, that follows the same profile as the excitation current. Other researchers have also found similar results in pressure built-up during cell cycling. For example, Schmitt et al. [18] found a 5 Pa of pressure rise at the beginning of the cycling with a bespoke prismatic cell and this was followed by an accumulative pressure pattern dependent on variations in cell temperature. However, a decrease of 40 mbar in the pressure, compared to that is at discharging stage, was observed after each 20-cycle period. This illustrates the stages where the cycling was stopped to perform the RPT testing to better understand the performance and degradation characteristics of the instrumented cells, as discussed in Section 3.2. However, no significant change in the pressure inside the cells was observed during RPT testing. Thus, the gas pressure inside the cells remained during the 100 cycles even through the cycling has been repeatedly interrupted for the RPT characterisation.

As highlighted in Fig. 6, the transient pressure measurements vary with the surface temperature changes during the charging and discharging periods (correlation between temperature and pressure is further discussed in Section 3.5). However, over the 100 cycles period, the mean value of the gas pressure increased, whereas the average temperature was essentially stable. Therefore, it is concluded that the variation in temperature cannot be the reason of the pressure rise during ageing. This is thought to be due to the accumulation of gas due to cell ageing. Comparing the gas pressure inside the cells before and after 100 cycles, a notable pressure built-up was found to be 105 mbar, 114 mbar and 52 mbar for *Cell 1*, *Cell 2* and *Cell 3* respectively.

Comparing the pressure accumulation inside the cells, a variation in the pressure behaviour of each individual cell was observed during the 100 cycles. Even though all the cells were instrumented in identically same way and with the same environmental conditions, a pressure difference of 9 mbar was observed between *Cell 1* and *Cell 2*, whereas a 53-mbar difference was observed between *Cell 1* and *Cell 3*. These are probably due to time differences between the instrumentation of each cell, further investigation of this phenomena is the subject of further work.

The evaluation of the irreversible behaviour of gas pressure was validated with a long period of resting (120 h) after the cycling. As highlighted in Fig. 7, internal gas pressure was stable over the testing time of 120 h. A drop of 21 mbar, 16 mbar and 26 mbar in gas pressure was observed for *Cell 1*, *Cell 2* and *Cell 3* respectively. These results show that gas pressure accumulation inside the cylindrical cells is deemed to be irreversible and does not decay during periods of cell relaxation after extended operation.

3.5. Gas pressure changes dependent on the ambient temperature

Under no-load conditions, the effects of ambient temperature on the gas pressure were investigated to separate the gas pressure changes due to the influence of the temperature from other effects. Fig. 8 demonstrates the relationship between gas pressure and the cell surface temperature. According to the ideal gas law defined in (Eq. (1)), a linear

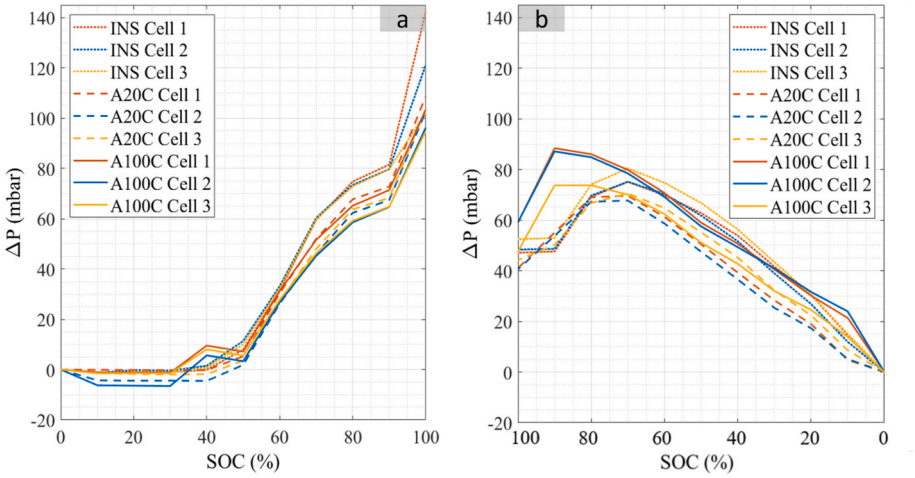

Fig. 5. Internal gas pressure of instrumented cells with respect to 0% SOC during the processes of (a) charging with C/3 rate and (b) discharging with 1C rate at different ageing stages (INS, A20C and AC100C refer to after instrumentation, 20 cycles and 100 cycles, respectively).

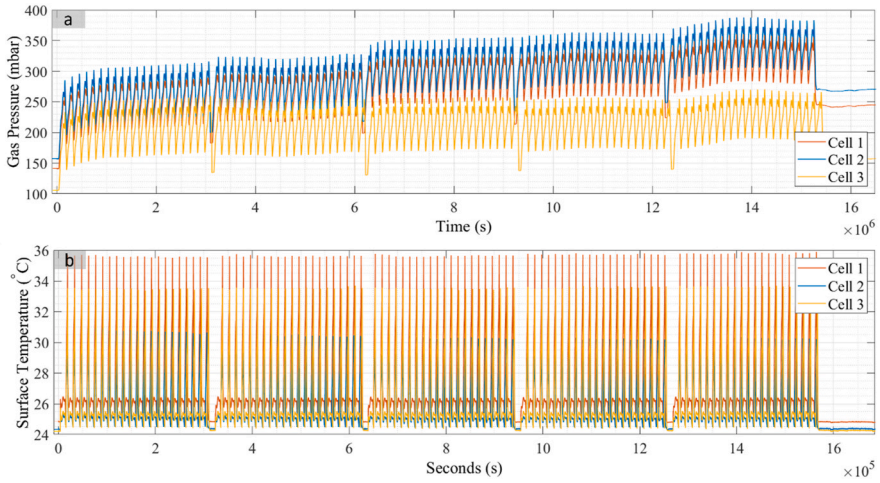

Fig. 6. (a) Internal gas pressure and (b) cell surface temperature changes over 100 cycles.

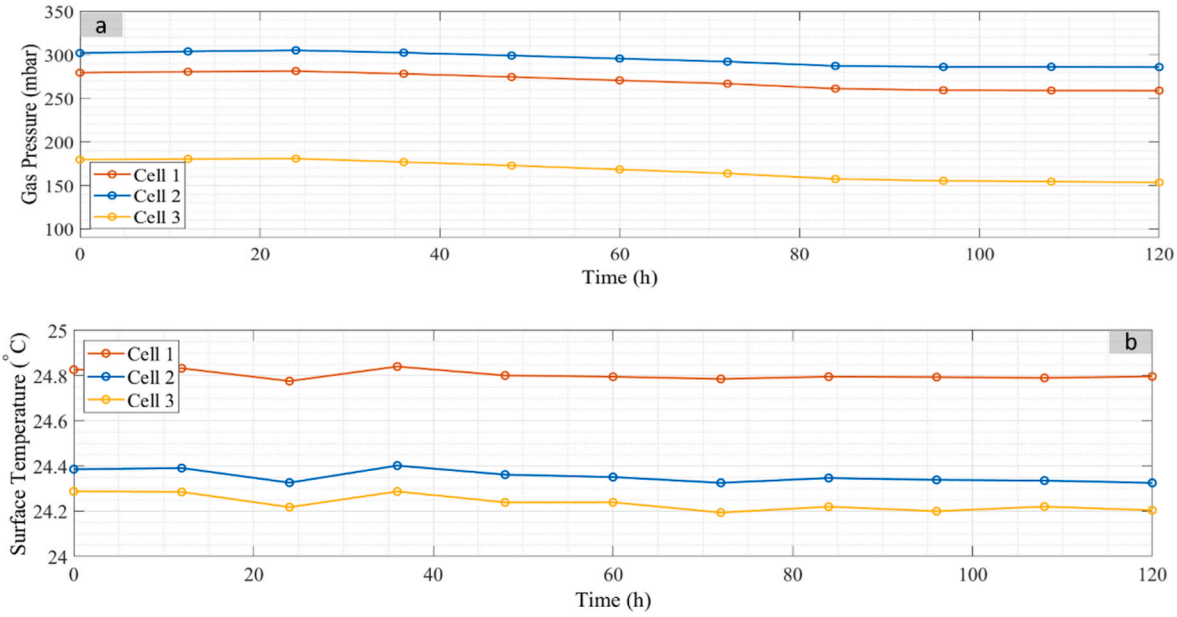

Fig. 7. The variation in (a) internal gas pressure and (b) surface temperature during 120 h resting after 100 cycles.

dependence of gas pressure on temperature is expected during the temperature profile testing. For each temperature level, the gas pressure inside the cells was measured after a resting period of 12 h, where the pressure reached steady-state values. The measurement points are marked with a black arrow in Fig. 8(a). However, the pressure measurements have not reached equilibrium when the highest temperature level of 55°C was applied to the cells. The underpinning reason by the gas pressure was unable to reach steady state when the ambient temperature was high is uncertain. Further work is required to quantify the time to reach equilibrium and how this value varies as a function ambient temperature, atmospheric pressure and the electrochemical composition of the cell's electrode and electrolyte.

The pressure changes (ΔP) due to ambient temperature between each temperature level was calculated, and the measurements are tabulated in Table 2. The results show that the rate of pressure increase or decrease varies between each temperature level even though the temperature on the cell surface was constantly increasing or decreasing 10°C (±0.65°C). Comparing the rate of pressure increase or decrease, all cells have a nonlinear relationship with ambient temperature, which cannot be explained by solely a linear relationship between the two quantities from (Eq. (1)). Similar results were also found in other studies in the literature. Schmitt et al. also found that nonlinear behaviour between the gas pressure and temperature during a thermal testing that was performed at open-circuit condition [18]. They also discovered the nonlinearity between the gas pressure and temperature increases with increasing levels of cell aging. This was attributed to the irreversible electrode swelling, resulting in a higher sensitivity to pressure or temperature changes [18]. However, the gas pressure increase depending on temperature was found to be reversible for both studies.

4. Further work

Further work is required to extend this research into instrumented cells to cover the advanced characterisation of cells and the possible deployment of instrumented cells within future battery systems for transport and intelligent stationary storage applications.

It is noteworthy that the aim of this initial study was to develop the underpinning methodology to measure internal gas pressure within the cell as a precursor to further work investigating how the accumulation of gas pressure varies as a function battery SOH and in particular if there is

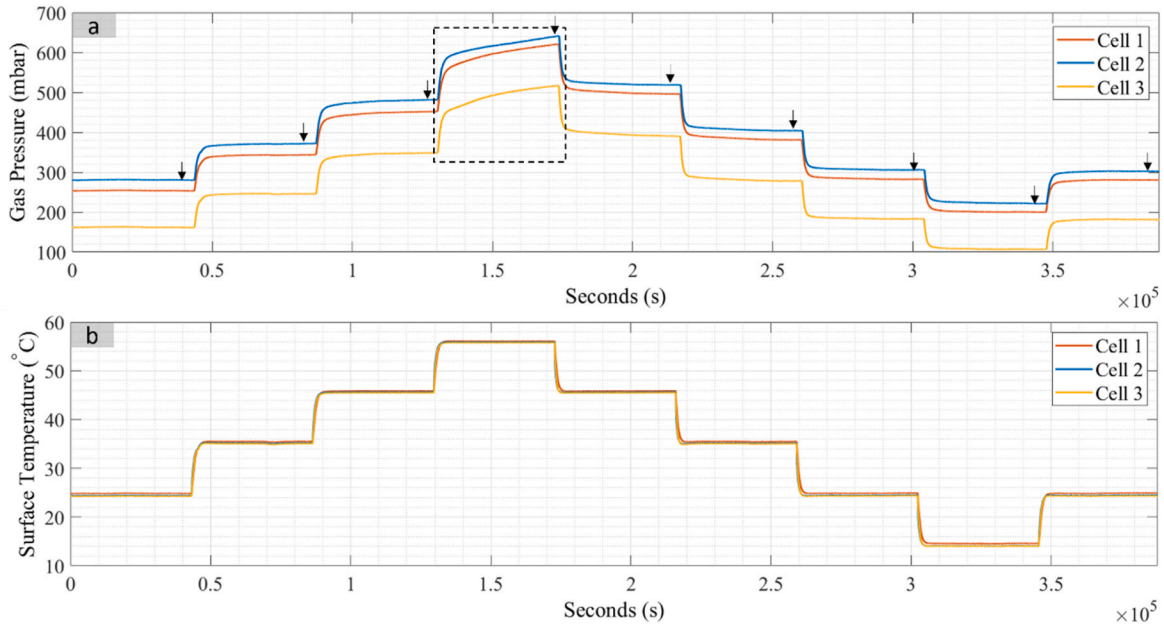

Fig. 8. (a) Internal gas pressure changes of the instrumented cells during (b) temperature profile testing.

Table 2
Increase in gas pressure during temperature profile testing (positive values in the table indicate the pressure increases whereas negative values are shown the pressure decreases).

ΔP (mbar)	Temp. (°C)							
	25°C → 35°C	35°C → 45°C	45°C → 55°C	55°C → 45°C	45°C → 35°C	35°C → 25°C	25°C → 15°C	15°C → 25°C
Cell 1	+90.83	+108.35	+168.27	−124.31	−115.04	−98.82	−82.58	+88.80
Cell 2	+92.16	+110.81	+158.26	−122.06	−115.01	−98.22	−84.70	+81.36
Cell 3	+84.62	+102.82	+168.43	−126.39	−112.40	−95.05	−76.46	+74.57

any corelation with specific degradation modes, often defined in the literature as a loss of active material (LAM) or Loss of Lithium Inventory (LLI) [1].

Our initial results highlighted a variation in pressure accumulation between instrumented cells. These are probably due to time differences between the instrumentation of each cell. Further research is required to investigate the environmental effects on the instrumentation process. This is important to understand given the minor changes in gas pressure that have been observed during cell operation. Authors have confidence in the validity of the experimental results presented. We aim to continue our instrumented cell development, increasing the sample size of cells evaluated. This will be achieved through the automated low volume manufacturing of instrumented cells, to strengthen our statistical evidence and experimental repeatability.

The transferability of this in-operando monitoring method to different types of pressure sensors, cell formats, other chemistries and environmental conditions is also under investigation. Of particular interest is to better understand the correlation between gas accumulation and pressure variation for different cathode materials (e.g., Nickel Manganese Cobalt NMC vs Lithium Iron Phosphate) and electrolyte compositions. This could provide insightful data to better understand the correlation between gas pressure accumulation and SOH or battery safety. Moreover, further research will be to investigate the gas pressure inside the cell under abuse conditions and variations in atmospheric pressure. However, this will change the sensor and fitting design to integrate our in-situ monitoring method for thermal runaway conditions. Further research is required to assess the suitability of the sensors and cell engineering/sealing techniques when quantifying cell performance under extreme use cases, such as overcharge, undercharge, higher ambient temperatures or mechanical excitation.

In addition to the use of instrumented cells for advanced battery characterisation, the data presented will support future innovations in the parameterisation and validation of electrochemical models that aim to corelate the voltage response, heat generation and ageing within the cell to its internal structure, and the changes in material composition associated with both operation and storage.

5. Conclusion

Our systematic and rigorous methodology for cell modification, instrumentation and verification process [6] has been implemented to monitor the internal gas pressure changes during cell operation and ageing. We have evaluated the internal gas pressure due to formation cycles and post-manufacturing via a novel method of penetration testing. Our experimental results demonstrate that the performance and degradation characteristic of the lithium-ion cells are not adversely affected by instrumentation. The effect of SOC, degradation and temperature on gas pressure inside the cells was evaluated in this study. The results highlight, a nonlinear relationship between gas pressure and the SOC (%) levels during charging and discharging. Trends were obtained for the internal pressure changes dependent on SOC (%) increase during the charge and discharge processes, respectively. The internal pressure reached its highest value between 90% and 100% SOC for all cells during the charging stage, whereas that was between 90% and 70% SOC during discharging. Regarding the temperature correlation with the internal gas pressure, the nonlinearity between gas pressure and the temperature was quantified. This has become noticeable at higher ambient temperatures during temperature profile testing under no-load cell conditions. During the period of 100 cycles, we observed an irreversible pressure built-up inside the cells. The evaluation of the

irreversible behaviour of gas pressure was validated with a long period of resting (120 h) after the cycling. Our study highlights the importance of monitoring gas pressure during cell operation. Gas pressure could be employed as another indicator for the advanced characterisation of battery safety and degradation. Plus, in-situ gas pressure could be employed for enhanced battery diagnostics, and for developing electrochemical models to estimate the SOC and SOH of the LIBs for advanced monitoring and BMS control systems.

CRediT authorship contribution statement

B. Gulsoy: Formal analysis, Writing – original draft, designed test rigs, performed experiments, analysed the data and wrote the original manuscript. **T.A. Vincent:** Writing – review & editing, helped instrumentation activity and contributed reviewing the manuscript. **C. Briggs:** helped designing the penetration test rig. **J.E.H. Sansom:** Writing – review & editing, Supervision. **J. Marco:** provided research definition, Writing – review & editing, Supervision, reviewing manuscript.

Declaration of competing interest

The authors declare that they have no known competing financial interests or personal relationships that could have appeared to influence the work reported in this paper.

Data availability

The data generated and analysed during the current study are not publicly available for legal/ethical reasons but are available from the corresponding author on reasonable request.

Acknowledgements

This work was supported by the WMG High Value Manufacturing Catapult, Part-funded by Innovate UK, the Aerospace Technology Institute (Grant Number: TS/V028049/1) and the Faraday Institution Multi-Scale Modelling project (EP/S003053/1 grant number FIRG003).

References

[1] A. Matasso, D. Wetz, F. Liu, The effects of internal pressure evolution on the aging of commercial Li-ion cells, ECS Trans. 58 (46) (Apr. 2014) 37–44, https://doi.org/10.1149/05846.0037ECST/XML [Online]. Available, https://iopscience.iop.org/article/10.1149/05846.0037ecst. (Accessed 21 November 2022).

[2] J.K. Ostanek, W. Li, P.P. Mukherjee, K.R. Crompton, C. Hacker, Simulating onset and evolution of thermal runaway in Li-ion cells using a coupled thermal and venting model, Appl. Energy 268 (Jun. 2020), 114972, https://doi.org/10.1016/J.APENERGY.2020.114972.

[3] Z. Wei, J. Zhao, H. He, G. Ding, H. Cui, L. Liu, Future smart battery and management: advanced sensing from external to embedded multi-dimensional measurement, J. Power Sources 489 (Mar. 2021), https://doi.org/10.1016/J.JPOWSOUR.2021.229462.

[4] M. Clarke, J.J. Alonso, Lithium-ion battery modeling for aerospace applications, doi: 10.2514/1.C036209, https://doi.org/10.2514/1.C036209, 2021. (Accessed 2 December 2022).

[5] Y. Ding, Z.P. Cano, A. Yu, J. Lu, Z. Chen, Automotive Li-ion batteries: current status and future perspectives, 2019 21, Electrochem. Energy Rev. 2 (1) (Jan. 2019) 1–28, https://doi.org/10.1007/S41918-018-0022-Z [Online]. Available: https://link.springer.com/article/10.1007/s41918-018-0022-z. (Accessed 2 December 2022).

[6] B. Gulsoy, T.A. Vincent, J.E.H. Sansom, J. Marco, In-situ temperature monitoring of a lithium-ion battery using an embedded thermocouple for smart battery applications, J. Energy Storage 54 (Oct. 2022), 105260, https://doi.org/10.1016/J.EST.2022.105260 [Online]. Available: https://linkinghub.elsevier.com/retrieve/pii/S2352152X22012580. (Accessed 13 July 2022).

[7] J. Huang, S.T. Boles, J.M. Tarascon, Sensing as the key to battery lifetime and sustainability, 2022 53, Nat. Sustain. 5 (3) (Mar. 2022) 194–204, https://doi.org/10.1038/s41893-022-00859-y [Online]. Available: https://www.nature.com/articles/s41893-022-00859-y. (Accessed 2 December 2022).

[8] Z. Liao, et al., Experimental evaluation of thermolysis-driven gas emissions from LiPF6-carbonate electrolyte used in lithium-ion batteries, J. Energy Chem. 49 (Oct. 2020) 124–135, https://doi.org/10.1016/J.JECHEM.2020.01.030.

[9] Z.Y. Jiang, Z.G. Qu, J.F. Zhang, Z.H. Rao, Rapid prediction method for thermal runaway propagation in battery pack based on lumped thermal resistance network and electric circuit analogy, Appl. Energy 268 (2020), 115007, https://doi.org/10.1016/J.APENERGY.2020.115007. Jun.

[10] S. Atalay, M. Sheikh, A. Mariani, Y. Merla, E. Bower, W.D. Widanage, Theory of battery ageing in a lithium-ion battery: capacity fade, nonlinear ageing and lifetime prediction, J. Power Sources 478 (Dec. 2020), 229026, https://doi.org/10.1016/J.JPOWSOUR.2020.229026.

[11] M. Raghibi, B. Xiong, S. Phadke, M. Anouti, Role of the electrolyte in gas formation during the cycling of a Gr//NMC battery as a function of temperature: solvent, salt, and ionic liquid effect, Electrochim. Acta 362 (Dec. 2020), https://doi.org/10.1016/J.ELECTACTA.2020.137214.

[12] N. Zhang, H. Tang, Dissecting anode swelling in commercial lithium-ion batteries, J. Power Sources 218 (Nov. 2012) 52–55, https://doi.org/10.1016/J.JPOWSOUR.2012.06.071.

[13] D.P. Finegan, et al., Characterising thermal runaway within lithium-ion cells by inducing and monitoring internal short circuits, Energy Environ. Sci. 10 (2017) 1377, https://doi.org/10.1039/c7ee00385d.

[14] Y. Jia, J. Darst, A. Surelia, D. Delafuente, D. Finegan, J. Xu, Deformation and fracture behaviors of cylindrical battery shell during thermal runaway, J. Power Sources 539 (Aug. 2022), https://doi.org/10.1016/J.JPOWSOUR.2022.231607.

[15] A. Matasso, D. Wong, D. Wetz, F. Liu, Correlation of bulk internal pressure rise and capacity degradation of commercial LiCoO 2 cells, J. Electrochem. Soc. 161 (14) (Sep. 2014) A2031–A2035, https://doi.org/10.1149/2.0221414JES/XML [Online]. Available: https://iopscience.iop.org/article/10.1149/2.0221414jes. (Accessed 21 November 2022).

[16] A. Schiele, T. Hatsukade, B.B. Berkes, P. Hartmann, T. Brezesinski, J. Janek, High-throughput in situ pressure analysis of lithium-ion batteries, Anal. Chem. 89 (15) (Aug. 2017) 8122–8128, https://doi.org/10.1021/ACS.ANALCHEM.7B01760/SUPPL_FILE/AC7B01760_SI_001.PDF [Online]. Available, https://pubs.acs.org/doi/abs/10.1021/acs.analchem.7b01760. (Accessed 21 November 2022).

[17] S. Schweidler, L. De Biasi, A. Schiele, P. Hartmann, T. Brezesinski, J. Janek, Volume changes of graphite anodes revisited: a combined operando X-ray diffraction and in situ pressure analysis study, J. Phys. Chem. C 122 (16) (Apr. 2018) 8829–8835, https://doi.org/10.1021/ACS.JPCC.8B01873/SUPPL_FILE/JP8B01873_SI_001.PDF [Online]. Available, https://pubs.acs.org/doi/abs/10.1021/acs.jpcc.8b01873. (Accessed 21 November 2022).

[18] J. Schmitt, et al., Measurement of gas pressure inside large-format prismatic lithium-ion cells during operation and cycle aging, J. Power Sources 478 (Dec. 2020), 228661, https://doi.org/10.1016/J.JPOWSOUR.2020.228661.

[19] J. Huang, et al., Operando decoding of chemical and thermal events in commercial Na(Li)-ion cells via optical sensors, 2020 59, Nat. Energy 5 (9) (Aug. 2020) 674–683, https://doi.org/10.1038/s41560-020-0665-y [Online]. Available: https://www.nature.com/articles/s41560-020-0665-y. (Accessed 30 August 2022).